

Current crustal deformation of the Taiwan orogen reassessed by cGPS strain-rate estimation and focal mechanism stress inversion

Sean Kuanhsiang Chen,¹ Yih-Min Wu,^{1,2} Ya-Ju Hsu³ and Yu-Chang Chan³

¹*Department of Geosciences, National Taiwan University, No. 1, Sec. 4, Roosevelt Road, Taipei 106, Taiwan. E-mail: drymwu@ntu.edu.tw*

²*National Center for Research on Earthquake Engineering, NARLabs, Taipei 10668, Taiwan*

³*Institute of Earth Sciences, Academia Sinica, No. 128, Sec. 2, Academia Road, Taipei 115, Taiwan*

Accepted 2017 April 24. Received 2017 April 20; in original form 2016 October 17

SUMMARY

We study internal deformation of the Taiwan orogen, a young arc-continental collision belt, which the spatial heterogeneity remains unclear. We aim to ascertain heterogeneity of the orogenic crust in depth when specifying general mechanisms of the Taiwan orogeny. To reach this goal, we used updated data of continuous GPS (cGPS) and earthquake focal mechanisms to reassess geodetic strain-rate and seismic stress fields of Taiwan, respectively. We updated the both data sets from 1990 to 2015 to provide large amount of constraints on surficial and internal deformation of the crust for a better understanding. We estimated strain-rate tensors by calculating gradient tensors of cGPS station velocities in horizontal 0.1° -spacing grids via Delaunay triangulation. We determined stress tensors within a given horizontal and vertical grid cell of 0.1° and 10 km, respectively, by employing the spatial and temporal stress inversion. To minimize effects of the 1999 M_w 7.6 Chi–Chi earthquake on trends of the strain and stress, we modified observational possible bias of the cGPS velocities after the earthquake and removed the first 15-month focal mechanisms within the fault rupture zone. We also calculated the Anderson fault parameter ($A\phi$) based on stress ratios and rake angles to quantitatively describe tectonic regimes of Taiwan. By examining directions of seismic compressive axes and styles of faulting, our results indicate that internal deformation of the crust is presently heterogeneous in the horizontal and vertical spaces. Directions of the compressive axes are fan-shaped oriented between $N10^\circ W$ and $N110^\circ W$ in the western and mid-eastern Taiwan at the depths of 0–20 km and near parallel to orientations of geodetic compressional axes. The orientations agreed with predominantly reverse faulting in the western Taiwan at the same depth range, implying a brittle deformation regime against the Peikang Basement High. Orientations of the compressive axes most rotated counter-clockwise at the depths of 20–40 km, coinciding with transition of styles of faulting from reverse to strike-slip faulting along the depths as revealed by variation of the $A\phi$ values. The features indicate that internal deformation of the upper crust is primarily driven by the same compressional mechanism. It implies that geodetic strains could detect the deformation from surface down to a maximal depth of 20 km in most regimes of Taiwan. We find that heterogeneity in orientations of compressive axes and styles of faulting is strong in two regimes at the northern and southern Central Range, coinciding to areas of the orogenic thinned/thickened crust. Conversely, the heterogeneity is weak in the central Western Foothills at surrounding area of root of the overthickened crust. This observation, coupled with regional seismological observations, may imply that vertical deformation from crustal thickening and thinning and thinning-related dynamics from mantle flows may have joint influence on degree of stress heterogeneity.

Key words: Plate motions; Satellite geodesy; Earthquake source observations; Kinematics of crustal and mantle deformation.

1 INTRODUCTION

Plate convergence concerns continental or continental-oceanic lithospheric collision in complex orogeny then creates orogens along

the plate boundaries. The Taiwan orogen is a young arc-continental collision product has been created since 3–5 Ma (Teng 1990). The collision resulted from convergence between the Eurasian and Philippine Sea plates at a rapid rate of $\sim 82 \text{ mm yr}^{-1}$ in 310°

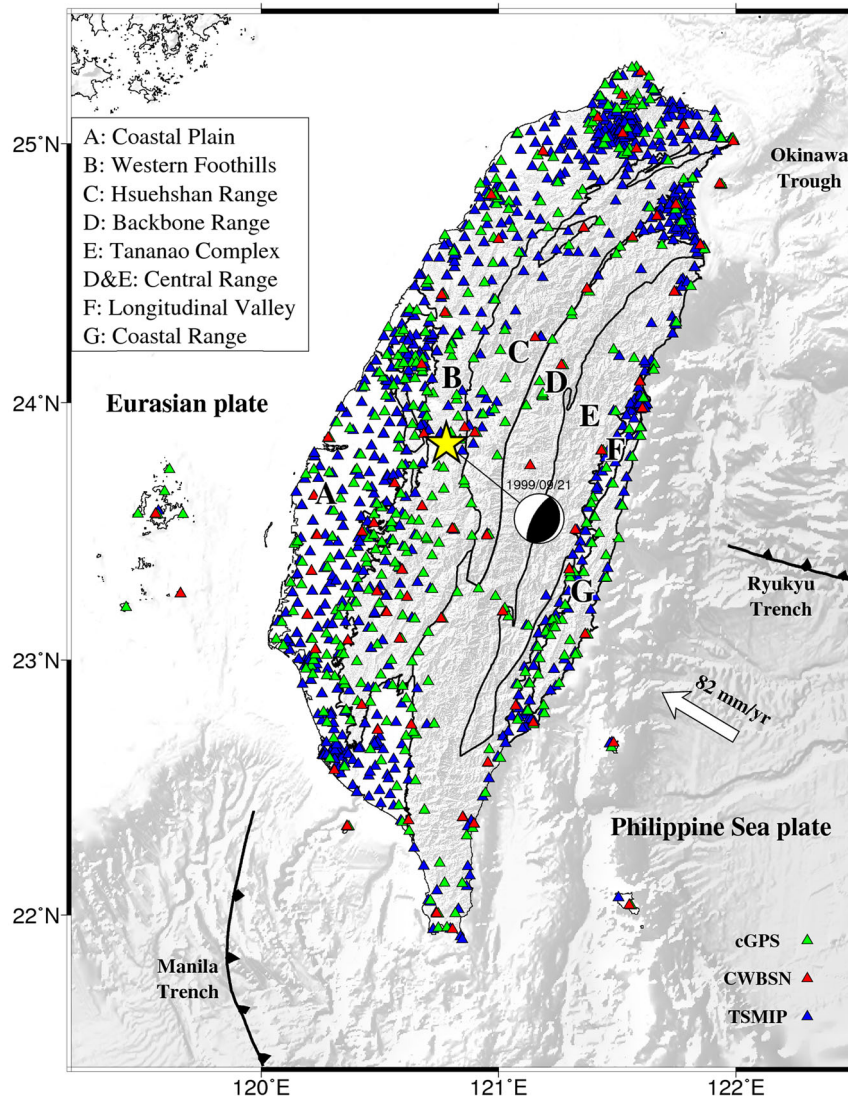


Figure 1. Station distributions, plate kinematics and tectonic settings of the study area. Integrated cGPS and seismic networks are coloured in different triangles. cGPS: continuous GPS sites; CWBSN: Central Weather Bureau Seismic Network and TSMIP: Taiwan Strong Motion Instrumentation Program. Major geological provinces on the Taiwan orogen are marked by black curves and labeled from A to G. The yellow star and the black beach ball represent epicentre and nodal planes of the 1999 Chi-Chi earthquake, respectively.

orientation (Yu *et al.* 1997; Hsu *et al.* 2009, Fig. 1) which is consumed by the orogeny and two nearby subductions. To the south of the Taiwan orogen, the Eurasian plate subducts eastward beneath the Philippine Sea plate. In contrast, to the east, the Philippine Sea plate subducts northward beneath the Eurasian plate. Regarding the orogen as a collision zone, debate associated with internal deformation of the orogenic crust is homogeneous or heterogeneous remains unresolved. In the past three decades, the Taiwan orogeny is considered that the kinematic mechanism may be explained by two end-member models. The thin-skinned model (Suppe 1981) defined the entire orogeny as above a pre-existing lithospheric detachment, and the deformation did not include materials below the detachment. Another view, the thick-skinned model (Wu *et al.* 1997) proposed the full lithosphere participates in the orogeny without a required detachment. To date, the rapid convergence rate across the two plates in Taiwan has created several geological provinces (see Supporting Information), over 3 km mountain ranges from the sea level and frequent seismic activity. The active orogeny provided a

best place for the establishment of geodetic and geophysical monitoring systems to investigate internal deformation of the orogen and verify the end-member models.

Over the last two decades, a large amount of continuous GPS (cGPS) observations in Taiwan region (Fig. 1) have enabled quantification of surface deformation (Yu *et al.* 1997; Hsu *et al.* 2009; Ching *et al.* 2011b). At the same time, dense seismic networks (Fig. 1) from the Central Weather Bureau Seismic Network (CWBSN) and the Taiwan Strong Motion Instrumentation Program (TSMIP) have enabled inversions of seismic deformation in the orogen. Recent states of geodetic strain and seismic stress at Taiwan have been estimated from gradients of GPS station velocities (Bos *et al.* 2003; Lin *et al.* 2010) and principal axes of earthquake focal mechanisms (Kao & Jian 2001; Wu *et al.* 2008b; Wu *et al.* 2010b), respectively. Few studies have jointly analysed the states of geodetic strain and seismic stress (Chang *et al.* 2003; Hsu *et al.* 2009) to know relationship between the surface deformation and internal deformation of the crust. The both studies shown the two deformation

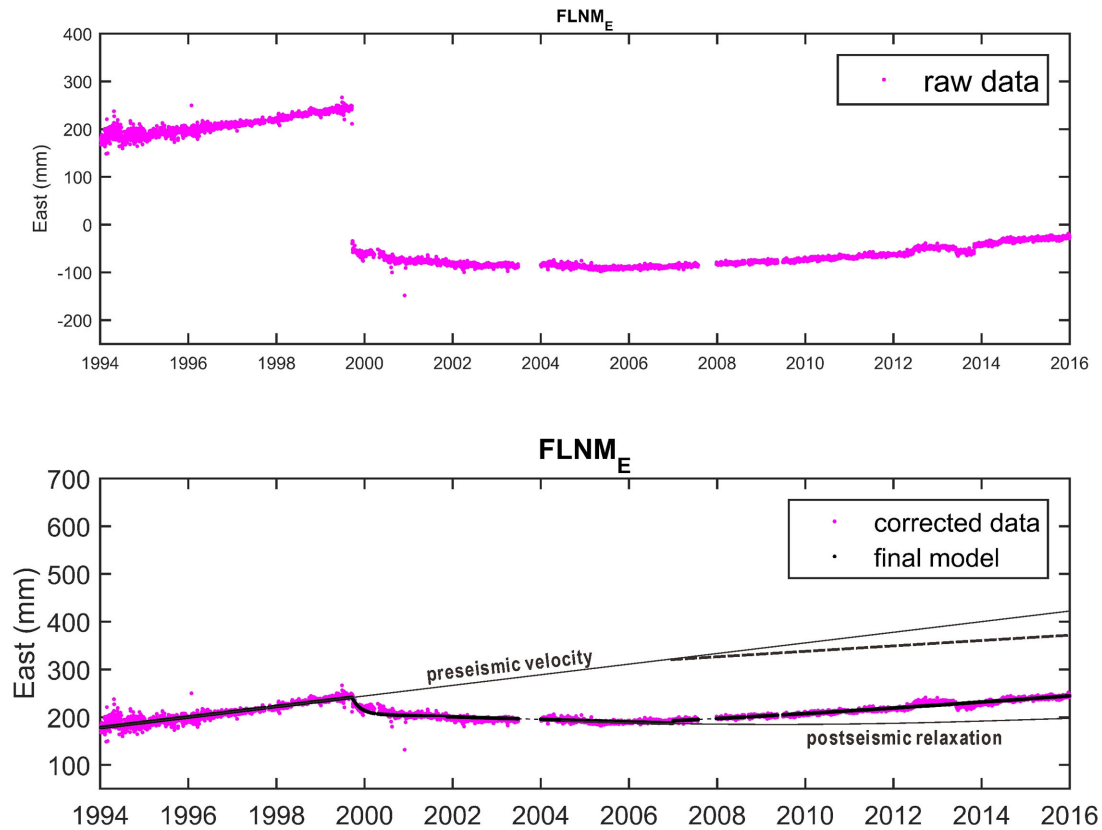


Figure 2. East component of position time-series of the FLNM cGPS site. Purple dots show the raw data and the corrected data without coseismic displacements. Black thick solid lines show the regression. The dashed line represents the velocity after 2007, indicating a possible observational bias in the trend (see the main text).

fields are azimuthal agreement and suggested a homogeneity of the crust is independent of depth. However, the agreement had a major deficiency of lack of vertical resolution because an average deformation field in the entire seismogenic crust was available at that time. The deficiency in resolution resulted from the early data set did not have sufficient amount of earthquake focal mechanism to determine stress tensors at depths.

The inferred homogeneity of the crust during the Taiwan orogeny was supported by the results from seismic anisotropy derived from teleseismic shear waves (Rau *et al.* 2000) and regional earthquake *P* waves (Kuo-Chen *et al.* 2013). Seismic anisotropy of crust may reflect aligned cracks or layered bedding in sedimentary rocks, or highly foliated metamorphic rocks. The aligned structural fabrics can help us determine state of stress in the crust, which are aligned with their flat faces oriented in direction of the minimum compressive stress. However, results from seismic anisotropy may be strongly rely on depth-dependent resolution capabilities. Recent seismic anisotropy studies (Huang *et al.* 2015; Koulakov *et al.* 2015) indicated that the Taiwan orogeny is layered deformation in the main collision zone (central to southern Taiwan), and the deformation is considered a product of two different kinematic mechanisms (Huang *et al.* 2015). The findings have provided progressive insights for the arc-continental collision and also motivated us to reassess internal deformation of the orogenic crust. We aim to ascertain the internal deformation whether the homogeneity is independent of depth when specifying general mechanisms of the Taiwan orogeny. To reach this goal, sufficient geodetic and seismic observations is crucial to the data coverage on the surface and in the entire crust.

2 DATA AND METHODS

Thanks to well-developed cGPS and seismic networks in the Taiwan region, we are able to use abundant data of the positions and the *P*-wave first arrivals. Large amount of the data can quantitatively estimate geodetic velocity field and nodal planes of earthquake focal mechanisms and obtain the strain-rate and stress fields, respectively. To obtain a high-resolution geodetic velocity field, we used the observations from 425 cGPS sites around the Taiwan region (Fig. 1) from 1994 to 2015 that were collected by the Institute of Earth Sciences, Academia Sinica. We processed the cGPS data with Bernese software, version 5.0 (Dach *et al.* 2007) using the double-difference phase observable and the tropospheric and ionospheric modeling. In Bernese v5.0 processing, seven surrounding International GPS Service (IGS) sites and twelve local cGPS sites of the Taiwan region (Fig. S1, Supporting Information) with sufficiently long observations are constrained to their 2008 International Terrestrial Reference Frame (ITRF2008, Altamimi *et al.* 2011) coordinates produce the coordinates of the other cGPS sites. To accurately estimate the trend of station velocity, we corrected displacements of the position time-series associated with the antenna changes and the co- and post-seismic movements. This study included longer cGPS observations and many more sites of Taiwan than the previous studies (Yu *et al.* 1997; Hsu *et al.* 2009; Ching *et al.* 2011b), which have enabled uncertainty minimization in the velocity field. However, the long observations may have involved a possible observational bias in some of station velocities (Fig. 2) resulted from the 1999 M_w 7.6 Chi–Chi earthquake at Taiwan (Fig. 1). The Chi–Chi earthquake ruptured along the Chelungpu fault and resulted in significant

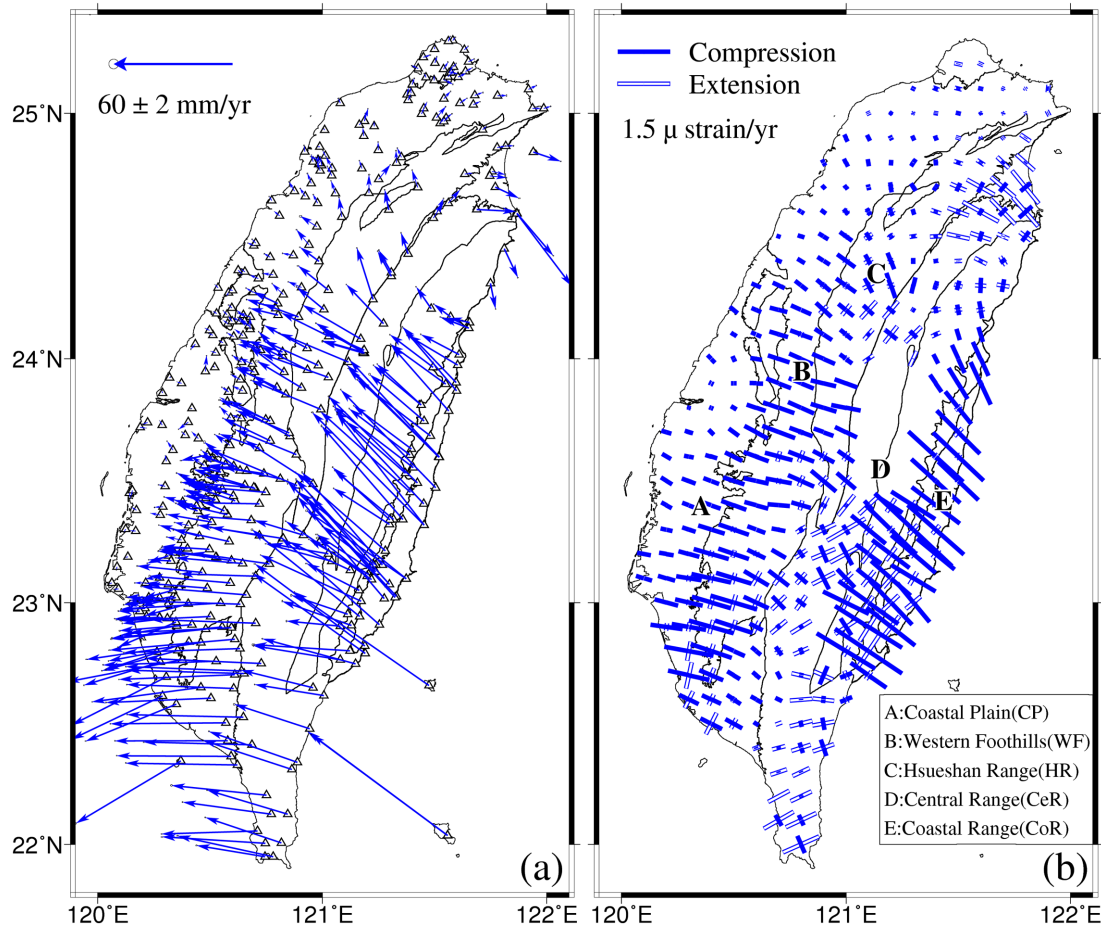


Figure 3. (a) cGPS velocity field of a 21 yr average in the Taiwan region. cGPS velocities refer to the S01R station (see Fig. S1, Supporting Information). Blue vectors are station velocities with a 95 per cent confidence ellipse. (b) Principal axes of geodetic strain rates. Amplitudes and orientations of the principal strain rates are shown in blue solid (compression) and hollow (extension) bars, respectively.

co- and post-seismic slips in the central Taiwan (Yu *et al.* 2003). Rousset *et al.* (2012) have modeled the post-seismic cGPS observations in the near- and far-field sites, but their results cannot explain well the later post-seismic observations. Our latest observations might reveal a linear velocity change (Fig. 2) which was considered a tectonic velocity change after main shock (e.g. Nikolaidis 2002); this change cannot be simply excluded by only considering the afterslips or relaxation (Rousset *et al.* 2012). Because the previous studies (Yu *et al.* 1997; Hsu *et al.* 2009) only used data of Taiwan before the Chi–Chi earthquake, this effect does not exist in their results. Ching *et al.* (2011b) used data of Taiwan from 1999 to 2005 but they used the data from the central Taiwan before the earthquake to avoid this regional effect. To minimize the effect on cGPS station velocities, after removing the post-seismic movements, we examined 17 cGPS sites recorded prior to the Chi–Chi earthquake. We found that seven of them may have the bias where are mostly located in the central Taiwan, and modified their post-seismic velocities by contrasting with their pre-seismic velocities. Additionally, we quantitatively estimated distribution of time-correlated noises on position time-series (Chen *et al.* 2014) and minimized the annual and semi-annual movements to obtain the station velocities. Taking all of the procedures into account, the standard deviations of cGPS velocities of a 21 yr trend are from 0.1 to 0.8 mm yr⁻¹ (Fig. 3a). By using the updated cGPS velocity field, we estimated the plane strain

tensors (Fig. 3b) by the approaches of Hsu *et al.* (2009). To know detailed variation of the strain field, we employed the Delaunay triangulation, a different method from Hsu *et al.* (2009), to interpolate the velocity by considering the observed horizontal velocities and data covariance. We interpolated the horizontal velocities to calculate gradient tensor of horizontal 0.1°-spacing grids and thus the gradients can be used to estimate strain-rate tensors (Hsu 2004). We excluded the strain-rate tensors where have been estimated in poorly constrained areas to avoid misleading interpretations. To verify the stability of strain-rate tensors, we used random removal of 10 per cent of station velocities that is conducted independently of each geological province to avoid irregular coverage in the horizontal areas. The tests over 50 iterations show the cGPS site coverage influenced the amplitude of strain rate more than the orientation but not very significant. We provided three examples of the tests for the verification (Fig. S2, Supporting Information). Taking the above procedures into account, the standard deviations of estimates of the amplitudes and orientations are 0.27 μ strain yr⁻¹ and 5°, respectively.

Due to strain data of Taiwan at the depths is presently few, it is being substituted for stress data can be determined simply by earthquake focal mechanisms (Kao & Jian 2001; Chang *et al.* 2003; Wu *et al.* 2008b, 2010a,b; Hsu *et al.* 2009). To know how directions of stresses vary in depth, data sets of focal mechanism in Taiwan

region are updated from 1991 to 2015 to increase the data coverage in the crust. We determined focal mechanisms by a genetic algorithm (Wu *et al.* 2008b) using data of *P*-wave first-motion polarities derived from the CWBSN, the TSMIP and Japan Meteorological Agency (JMA). However, as aforementioned, effect of the Chi–Chi earthquake on states of geodetic strain should be considered here. States of stresses in the seismogenic crust could vary significantly due to the coseismic stress change and afterslip. The variations in time, after the Chi–Chi earthquake, have been reported by several studies (Hsu *et al.* 2009, 2010; Wu *et al.* 2010b; Chan *et al.* 2012), and it was also observed after great earthquakes worldwide (e.g. Wesson & Boyd 2007; Hasegawa *et al.* 2012; Yoshida *et al.* 2012). We found that the stresses within the fault rupture zone (Lee *et al.* 2006) have changed the pre-seismic directions in the early post-seismic period and then gradually switched themselves back to the pre-seismic directions. To minimize this effect, we removed the first 15-month focal mechanisms following the Chi–Chi earthquake within the fault rupture zone. We selected the interval of 15 months because it has included a majority of the amplitude of cumulative afterslip (Hsu *et al.* 2007) and the observational aftershock amount (Wu & Chen 2007). After removing the regional focal mechanisms, a total of 7939 events are reserved (Fig. 4) and the parameters are listed in Table 1. We highlighted the key parameters below: standard deviations of the strike, dip and rake are about 15° , 14° and 20° , respectively. Quality factor (Q_{fp}) are 1.52 and 1.89 in the mean and standard deviation, respectively. Depth range of the focal mechanisms is between 0.5 and 275 km with a majority less than 20 km and the most less than 40 km (Fig. S3, Supporting Information).

We determined stress tensors from the surface to 40 km depth by considering earthquake location uncertainty in our data set to provide suitable grid size for the stress tensor inversion. By combining the *P*- and *S*-wave arrival times from the CWBSN, TSMIP and JMA sites, Wu *et al.* (2008a) provided an earthquake relocation catalogue have enhanced accuracy and reliability in the locations by comparing to the normal CWB locations. The location errors in longitude, latitude and depth were estimated approximately 3.1 ± 2.7 , 1.3 ± 1.6 and 4.6 ± 3.9 km, respectively, for the inland locales (Wu *et al.* 2013). Based on data set of focal mechanisms in this study was updated from that earthquake relocation catalogue (Wu *et al.* 2008a), we determined the stress tensors within a given horizontal and vertical grid cell of 0.1° and 10 km, respectively. We employed the spatial and temporal stress inversion (SATSI) algorithm (Hardebeck & Michael 2006) to invert the stress tensors. We permitted at least 10 focal mechanisms within the given grid cell for the inversion and searched focal mechanisms within an area twice the grid cell for grid nodes where focal mechanisms are insufficient. If the numbers of focal mechanism are still below the threshold, the grid nodes will be excluded from the inversion. We display the numbers within each grid cell in Fig. S4 in the Supporting Information. To verify results from the inversion are reliable in each grid cell, we applied a bootstrap algorithm to resample the observed focal mechanisms (Hsu *et al.* 2009). The 95 per cent confidence interval of principal stress axes at each depth are generally similar to the previous results derived from an earlier focal mechanism data set (Wu *et al.* 2010b). In addition, we used the Anderson fault parameter, $A\phi$ (e.g. Hardebeck & Hauksson 2001), to quantitatively describe tectonic regimes based on stress ratios and rake angles. $A\phi = (n + 0.5) + (-1)^n \times (R - 0.5)$, where $n = 0, 1$ and 2 for normal, strike-slip and reverse types, respectively. R is the stress ratio [$R = (\sigma_1 - \sigma_2)/(\sigma_1 - \sigma_3)$]. $A\phi$ increases gradually from 0.0 to 1.0 for normal faulting, 1.0–2.0 for strike-slip faulting and 2.0–3.0

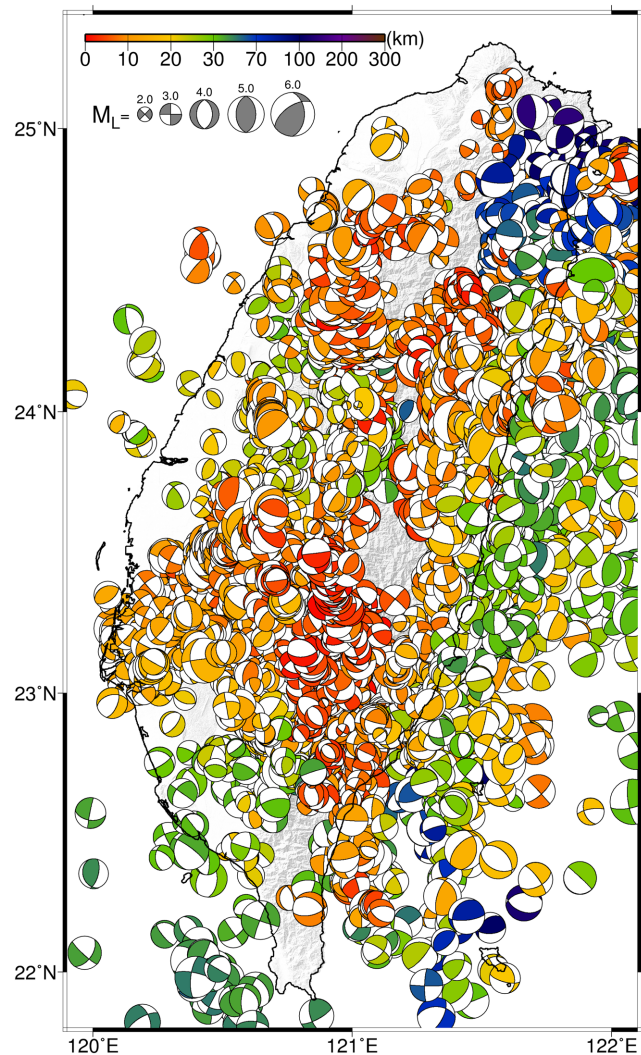


Figure 4. Final data set of earthquake focal mechanisms from 1991 to 2015 in the Taiwan region (see the main text). The magnitudes range from M_L 0.9 to 7.3. The nodal plane solutions and parameters are provided in Table 1.

for reverse faulting. To simplify the stress tensors in the horizontal 0.1° -spacing grids, we solely show horizontal projection of the σ_1 and σ_3 axes in each grid cell and mainly describe directions of the σ_1 axes.

To probe into heterogeneity in directions of the principal stress axes at depths and how the directions correlate to directions of geodetic strain axes, we compare orientations of stress axes to strain axes under an assumption. Since geodetic strain only constrained the surface and cannot be assumed to be constant at all depths (0–40 km), a direct comparison between strain and multilayered stresses is impracticable. We assume that internal deformation of the uppermost crust is a major signal in geodetic strain-rate observations. We thus compare orientations of compressive axes in the top layer (0–10 km) with orientations of compressional axes to examine their level of agreement. Orientations of compressive axes in the deeper layers are compared to the top layer to verify the orientations whether the heterogeneity is depth-dependent. For the agreement between orientations of the two axes, we give a threshold of within 20° divergence based on estimates of the strike, dip and rake have one standard deviation of 15° , 14° and 20° , respectively.

Table 1. Summary of the earthquake data used in this study and the uncertainties within stress tensor inversion.

Time period covered	1991 January 1–2015 December 31
Number of events	7939
M_L range	0.9–7.3
Longitude range	119.2°–124.7°
Latitude range	20.6°–25.5°
Depth range	0.5–275 km
Average standard deviation of strike	15.70
Average standard deviation of dip	14.37
Average standard deviation of rake	20.61
Average and standard deviation of Q_{fp}	1.52 ± 1.89
Standard deviation of strike at depths	15.61, 15.47, 16.03, 15.12
Standard deviation of dip at depths	15.75, 14.02, 13.60, 13.77
Standard deviation of rake at depths	22.24, 19.36, 18.97, 19.57
Average Q_{fp} at depths	1.36, 1.67, 1.51, 1.57

Note: Order of the values follows 10 km depth bins from surface to the depth of 40 km.

3 RENEWED GEODETIC STRAIN AND SEISMIC STRESS FIELDS OF TAIWAN AND THEIR SPATIAL RELATIONSHIP

In Fig. 3(b), we display a more precise geodetic strain-rate field than the previous studies (Bos *et al.* 2003; Chang *et al.* 2003; Hsu *et al.* 2009; Lin *et al.* 2010). The field shows general agreement with those studies on types of strain and orientations of strain axes. The agreement includes a predominantly strong compressional strain in the Western Foothills (WF) and Coastal Range (CoR), a predominantly extensional strain in the Central Range (CeR), a weak compressional strain in the Coastal Plain, a compressional to extensional strain transition in the Hsuehshan Range (HR) and a fan-shaped orientation of compressive axes towards 310° in most regimes (Fig. 3b). Our result has few disagreement with those studies as to regional features, for example, amplitudes of strain rates from this study are positive lower in the southernmost WF and CoR and negative lower in the southern CeR than from some of those studies. The disagreement may result from different station distributions in each study and the advantages and disadvantages of different methods. In Fig. 5, we display principal stress axes in four layers above the 40 km depth in the Taiwan region. In Fig. 6, we present first layered tectonic regimes of Taiwan in the corresponding stress grid cells of the Fig. 5. Map views of the principal stress axes show directions of the σ_1 axes at 0–10 km depths are fan-shaped oriented in the western Taiwan from N10°W to N110°W (Fig. 5). The fan-shaped orientations are like to extend to the 10–20 km depth, which are generally consistent with the directions of σ_1 axes estimated by using focal mechanisms in different depth ranges (Wu *et al.* 2008b, 2010a,b; Hsu *et al.* 2009). Coincidentally, the orientations are near parallel to orientations of geodetic compressional axes in the western Taiwan; it was explained by brittle deformation regime where the orogenic crust goes against a Peikang Basement High (e.g. Hu *et al.* 1996; Wu *et al.* 2007) located on the edge of the westernmost Taiwan orogen. A barrier of the Peikang High resulted in a fan-shaped oriented deformation field are perpendicular to trends of geological provinces on the surface. Result from the Anderson fault parameter show the $A\phi$ values are predominantly larger than 2.0, that is, reverse faulting, at the depths of 0–10 km in the western Taiwan (Fig. 6). Most of the $A\phi$ values are still larger than 2.0 when the depths go down to 20 km but they have no sufficient solutions in the northern areas. The pattern is similar to the previous result from the ratio of principal stress difference (ϕ) of Taiwan (Hsu *et al.* 2009), implying that σ_1 axes are horizontally directed in the western

Taiwan at depths due to plate convergence. Our results agreed with structural evolution of a brittle part of the crust which is caused by the barrier of the Peikang High under plate convergence. Furthermore, we can identify the brittle part of the crust with a probable 20 km depth from the surface in the western Taiwan that was unsure before. Note that we need to highlight a region of predominantly reverse faulting in the central WF. The region includes at least from the surface to the depth of 30 km (Fig. 6) and in an area with the size of 50 km × 30 km. This feature is unlikely an observational bias and will be discussed in the next section.

To the eastern Taiwan, directions of the σ_1 axes are general agreement at the depths of 0–20 km but they are heterogeneous in the horizontal space (Fig. 5). The directions show strong heterogeneity in the CeR, especially, in the northern to central segment. The σ_1 axes are near N45°E orientation in the northernmost CeR where are thought to be influenced by the rifting of the Okinawa Trough (e.g. Wu *et al.* 2008b; Huang *et al.* 2012). The axes rotated counter-clockwise from the latitude of N24.5°–N24° southward to near N50°W orientation at the end of northern CeR (Fig. 5). The rotation agreed with orientations of the regional compressive axes (Wu *et al.* 2009) and compressional axes (Chen *et al.* 2014). At here, the $A\phi$ values also show strong heterogeneity in the horizontal space, revealing a mixture of strike-slip and reverse faulting along the coast and a predominantly normal faulting far from the coast (Fig. 6). In the central CeR and the entire CoR (the mid-eastern Taiwan), directions of the σ_1 axes predominantly kept the N50°W orientations, as same as the 310° plate convergence, in the 0–20 km depths (Fig. 5). The $A\phi$ values revealed a predominantly normal faulting in the central CeR and a mixture of strike-slip and reverse faulting in the entire CoR (Fig. 6). The features indicate the oblique collision zone beneath the east coast of Taiwan as revealed by the previous seismotectonic studies (e.g. Wu *et al.* 2008b; Huang *et al.* 2012). In the southern CeR, we found that directions of the σ_1 axes and the $A\phi$ values at the depths of 0–20 km are strong heterogeneity in the horizontal and vertical spaces. The directions approximately oriented in the 310° plate convergence but they are not in well azimuthal agreement (Fig. 5), and the values revealed a mixture of normal and strike-slip faulting and a predominantly strike-slip faulting at the depths of 0–10 and 10–20 km, respectively (Fig. 6).

However, we find that the directions of the σ_1 axes most rotated in the depths of 20–40 km. In the western Taiwan, the directions of σ_1 axes rotated counter-clockwise over 20° in the southern HR (Fig. 5). The variation in orientations of the overall stress axes at the 20 km depth may imply that a possible change of styles of faulting in depth. We find that the $A\phi$ values gradually reduce to near and less than 2.0, that is, strike-slip faulting, in the southern HR below the 20 and 30 km depth, respectively (Fig. 6). The values may reveal the tectonic regimes in depth are mainly characterized by a transition from reverse to strike-slip faulting. To the eastern Taiwan, the NE-oriented σ_1 axes in the northernmost CeR counter-clockwise rotated significantly to NW/EW-oriented (Fig. 5). The depth-dependent heterogeneity in the orientations is also visible to the $A\phi$ values along the coast, revealing a transition from predominantly reverse faulting (0–20 km) to a mixture of reverse and strike-slip faulting (20–40 km; Fig. 6). Our results show another counter-clockwise rotation of σ_1 axes in the mid-eastern Taiwan (Fig. 5), but the rotation and heterogeneity in depth is not as significant as at the northernmost CeR. The rotation is consistent with the previous results from principal compressive axes (Wu *et al.* 2010b), suggesting the stress partitioning at depth is caused by rheological change. The $A\phi$ values revealed that the transition of styles of faulting, from a mixture of reverse and strike-slip faulting to predominantly strike-slip faulting, seems

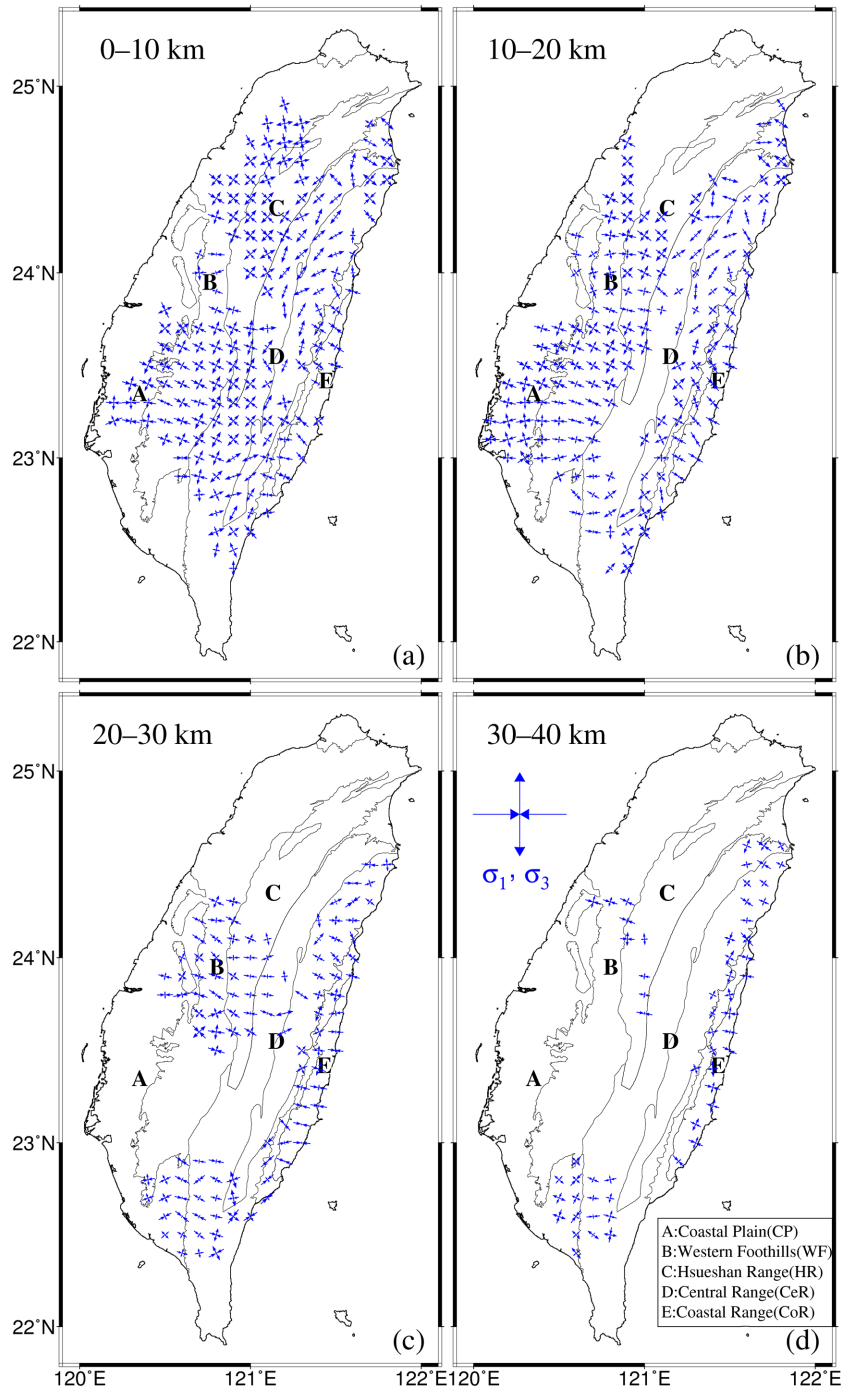


Figure 5. (a)–(d) Map view of orientations of principal stress axes from a 25 yr average in the Taiwan region. The layered depth is shown at the top-left corner of each map. The hollow grid nodes denote regimes with insufficient data for stress tensor inversion. Lengths of the stress axes projected to the surface are largest and close to zero when the plunges are 0° and 90° , respectively.

to occur at a deeper depth of 30 km (Fig. 6). Additionally, we find that directions of the σ_1 axes also seem to rotate counter-clockwise over 20° in the southern CeR (Fig. 5). The $A\phi$ values at the depths of 20–30 and 30–40 km revealed a transition from a mixture of reverse and strike-slip faulting to predominantly strike-slip faulting, respectively (Fig. 6). The heterogeneity in directions of stress and styles of faulting at the southern CeR is as significant as at the northernmost CeR. We will discuss the new features and possible implications in the next section.

In Fig. 7, we display a comparison of orientations of compressive axes in the top layer to orientations of compressional axes and to orientations of compressive axes in the deeper layers. Agreement is up to 71 per cent in terms of their overlaps. Agreement of orientations of compressive axes between orientations of compressive axes in the 0–10 km layer and compressional axes between the layers of 0–10 and 10–20 km in terms of the overlaps is 66 per cent which is similar to the level of Fig. 7(a). However, the agreement between the layers of 0–10 and 20–30 and 30–40 km dropped to the level of

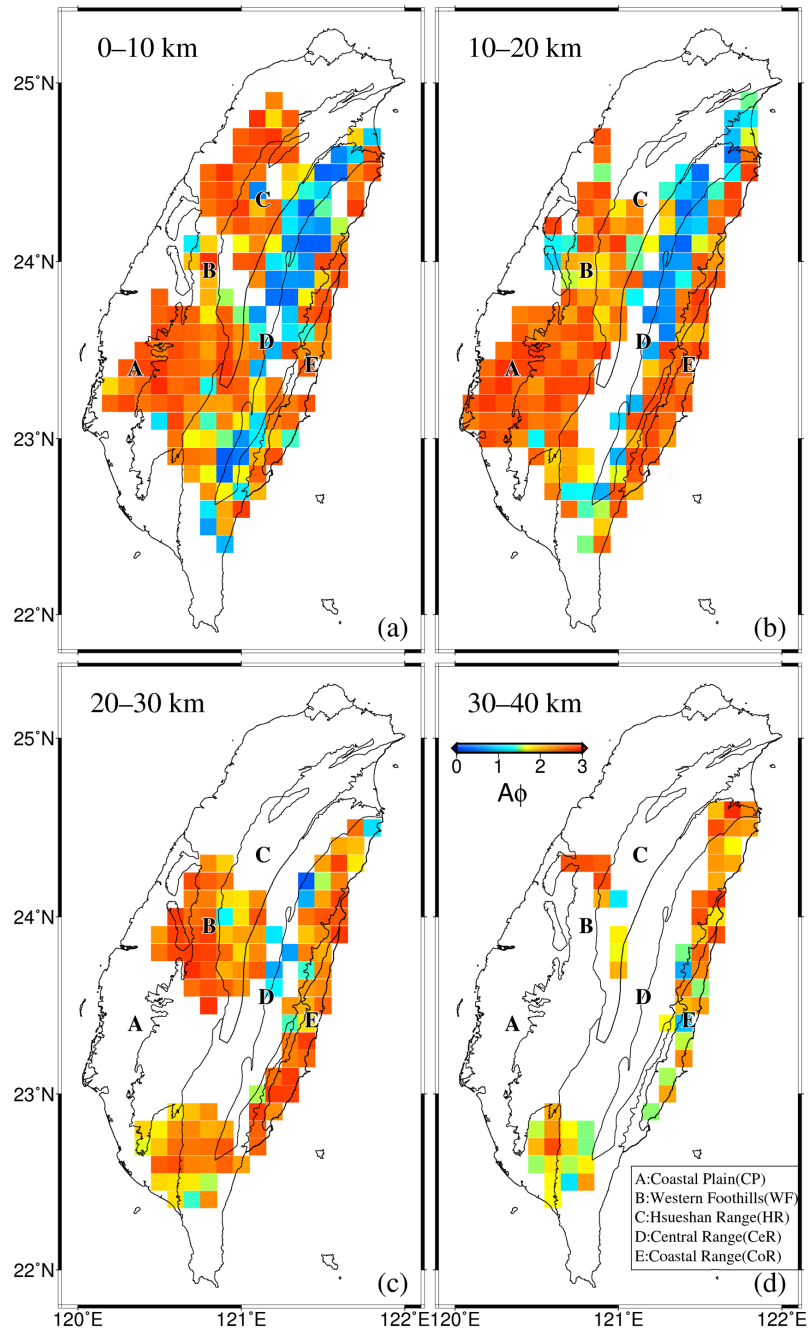


Figure 6. (a)–(d) The same as Fig. 5, but for tectonic regimes described by the Anderson fault parameter (A_ϕ). The regimes of reverse, strike-slip and normal faulting are shown in red, yellow to green and blue grids, respectively (see the main text).

42 and 21 per cent, respectively. Conversely, disagreement between orientations of compressive axes in the 0–10 km layer and compressional axes is limited in two areas: the northern and southern CeR (Fig. 7a). To verify the drop of levels of agreement in depth is not caused by the increase in data uncertainties with depth, we have examined the uncertainties in nodal plane solutions. In Table 1, we show the values of one standard deviation from strike, dip, rake and the values of average Q_{fp} in all depth bins. The standard deviations and Q_{fp} are larger and smaller, respectively, in the depths of 0–10 km and do not increase with depth. The result confirmed that the drop in depth is independent of data uncertainties; it may be due to the directions of stress axes at greater depths are spatially more distant from the shallowest depth, thus resulting in its more diversity. More

importantly, variation of level of the azimuthal agreement in depth revealed the stress heterogeneity in vertical space of Taiwan that was unknown before. Our results indicate that internal deformation of the orogenic crust of Taiwan is spatial heterogeneity that is depth-dependent, and are unlike to agree with inference of homogeneity of the crust (Chang *et al.* 2003; Hsu *et al.* 2009).

4 DISCUSSION

Worldwide studies have shown similar orientations of geodetic strain axes and seismic stress axes, for example, studies of southern California (Becker *et al.* 2005), Central Japan (Townend & Zoback

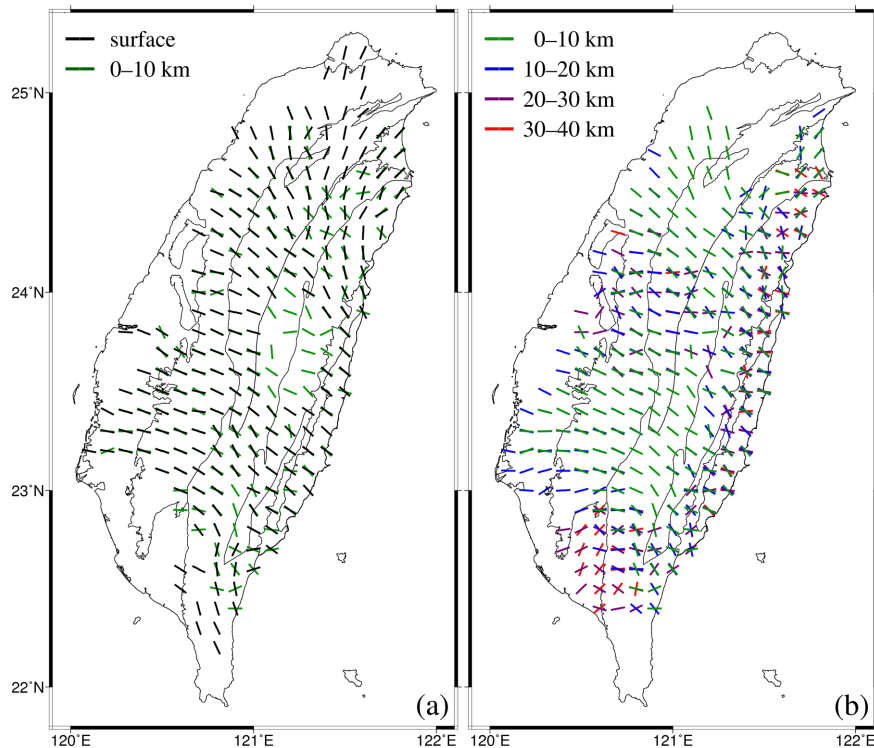


Figure 7. Comparison of orientations of (a) geodetic compressional and seismic compressive axes and (b) layered seismic compressive axes in the crust. The geodetic compressional axes are marked in black, and seismic compressive axes at various depths are shown in different colours.

2006), the Italian Peninsula (Palano *et al.* 2011, 2015), Iceland (Keiding *et al.* 2009) and the Tibetan Plateau (Wang *et al.* 2008). They inferred that both earthquakes and surface deformation are presently driven by the same tectonic mechanism. The inference is the same as the previous studies of Taiwan (Chang *et al.* 2003; Hsu *et al.* 2009) that lacked the vertical resolution resulting in a doubt of the same mechanism in the crust. Regarding recent studies of seismic anisotropy in Taiwan, a layered anisotropy is observed in the main collision zone by using ambient noise surface waves (Huang *et al.* 2015). The layered anisotropy shows near NS- and EW-orientated above and below the 10 km depth and is interpreted as collision-related compression and subduction-related shearing in the upper and lower crust, respectively. The proposed layered mechanism is supported by another 3-D anisotropy model derived from regional *P*-wave traveltimes (Koulakov *et al.* 2015). In the main collision zone, the *P*-wave azimuthal anisotropies are similar to that of Huang *et al.* (2015), but the perpendicular of NS- and EW-orientated anisotropies is proposed at the 20 km depth. In the eastern Taiwan, the *P*-wave azimuthal anisotropies are strongly NS-orientated below the 30 km depth where it is unresolved by the layered model (Huang *et al.* 2015). It is interpreted as a product of mantle displacements resulted from the oblique collision of the Philippine Sea plate (Koulakov *et al.* 2015). Our results demonstrated a similar pattern to the layered deformation in the main collision zone. In that upper crust, EW-oriented compressional and compressive axes agreed with NS-orientated anisotropy implying brittle deformation regime due to collision-related compression. To the lower crust, orientations of compressive axes are most rotated and styles of faulting transited from reverse to strike-slip faulting. The variations agreed with EW-orientated anisotropy and the implications of subduction-related shearing. The layered mechanism is not opposed to our basic observations even if the transition was inferred at two different depths from Huang *et al.* (2015) and Koulakov *et al.* (2015).

Our observations suggest that geodetic strains could detect internal deformation of the crust from surface down to a maximal depth of 20 km in the western and mid-eastern Taiwan. However, variation of orientations of stress axes and styles of faulting in depth implies that deformation below the upper crust is unable to be captured by geodetic strains.

Out of the main collision zone, disagreement between orientations of strain and stress axes in two regimes at the northern and southern CeR is of interest. We found that orientations of stress axes and styles of faulting are both strong heterogeneity in the horizontal and vertical spaces. The heterogeneities may be caused by vertical deformation associated with crustal thickening and thinning (Yang & Hauksson 2013); degree of the heterogeneities may be influenced by variation in the thickness of crust resulted in different dynamics of mantle flows (Lin & Kuo 2013). The Taiwan orogeny is currently experiencing crustal thinning, overthickened and thickening in the northern, central and southern regimes of Taiwan, respectively (Teng 1990; Wu *et al.* 1997). To the northern Taiwan, crustal thinning is driven by the horizontal lengthening associated with backarc rifting of the Okinawa Trough (Teng 1990; Wu *et al.* 1997). The rifting of the Okinawa Trough has affected styles of faulting in the northern Taiwan as a horizontally eastward transition from reverse to normal faulting (Hu *et al.* 2002; Wu, Kao *et al.* 2010). A thinned crust at about 30 km thickness within the northern Taiwan orogen has been inferred from seismic velocity structures (Kuo-Chen *et al.* 2012; Huang *et al.* 2014). Crustal thinning is apparent to normal faulting regime in the NE Taiwan at the 0–20 km depths (Fig. 6). In this depth range, strong heterogeneity in orientations of stress and styles of faulting in the horizontal space agreed with the thought of as a product of the vertical deformation of crust in crustal thinning regimes (Yang & Hauksson 2013). However, directions of the stress axes in the depths of 20–40 km rotated counter-clockwise toward NW/EW-oriented seem unlike a product of rifting of the

Okinawa Trough. The EW-oriented compressive axes are similar to regional shear wave azimuthal anisotropy (Kuo *et al.* 2012) that is considered a deformation field resulted from upper-mantle flows. The flows may come from a high Q -value mantle wedge with low viscosity and high temperature beneath the offshore NE Taiwan (Ko *et al.* 2012). The wedge may create different circulations to guide regional dynamics depend on thickness of the Eurasian crust derived from a scenario of 3-D mantle flow (Lin & Kuo 2013). Due to the wedge is bounded by the subducting Philippine Sea plate and a Eurasian thinned crust, it may have provided a channel for the mantle flow toward the west beneath the thinned crust. Westward intrusion of the mantle flow resulted from thinning-related dynamics by considering that scenario (Lin & Kuo 2013) might give rise to degree of the heterogeneity in styles of faulting on the overriding thinned crust. The westward intrusion can also explain a mixture of reverse and strike-slip faulting at the depths of 20–40 km. The regional observations may imply that vertical deformation from crustal thinning and thinning-related dynamics from mantle flows may have joint influence on stress heterogeneity.

To the southern Taiwan, crustal thickening is driven by the horizontal shortening associated with subduction of the Eurasian plate. Results from the thermokinematic model of the Taiwan orogen suggest that the underplating beneath the CeR sustain crustal thickening and exhumation (Simoes *et al.* 2007). Crustal exhumation in the southern CeR was verified by the rapid uplift rates, for example, an average of 9 mm yr^{-1} during the last 0.6 Ma (Liu 1982) and a maximum of 8 mm yr^{-1} at present (Ching *et al.* 2011a). The exhumation may be explained by gravitational collapse of the uppermost crust (Teng 1990; Hsu *et al.* 2009) and gravitational sinking of the Eurasian plate (Huang *et al.* 2015). Normal faulting regime in the depths of 0–10 km of the southern CeR (Fig. 6) and reverse faulting regime in the depths (20–30 km) may reveal the gravitational collapse and sinking, respectively. The pattern is similar to a recent study of focal mechanism analysis in the southern CeR (Chiang *et al.* 2016) implying the thickening of crust. Root of the thickened crust corresponding to the uplifted topography is inferred from different seismic-wave velocity structures (Wu *et al.* 2007; Kuo-Chen *et al.* 2012; Huang *et al.* 2014) and gravity-based density structures (Hsieh & Yen 2016). These studies suggest that the thickened crust reached an average depth of 30 km which is much shallower than the depth of 50 km in the central Taiwan as an overthickened crust. The not thick crust may be similar to the case in the northern CeR where the heterogeneity in orientations of stress axes and styles of faulting is strong at the regime of orogenic thin crust. Limited by few study associated with the underplating beneath the southern CeR, more observations are crucial for a better understanding of the heterogeneity. Additionally, regional agreement on reverse faulting in the central WF is obvious between the surface and the depth of 30 km. The agreement of a wide depth range coincided with a surrounding area of root of the overthickened crust inferred from seismic velocity structures (Kuo-Chen *et al.* 2012; Huang *et al.* 2014). It may imply that the overthickened crust have blocked mantle flows under the Philippine Sea oceanic crust toward the west (Lin & Kuo 2013), thus the flows may change toward the north. The change in direction of the mantle flows is supported by a strong NS-oriented anisotropy at depths near the eastern coast of Taiwan (Koulakov *et al.* 2015).

Our observations provide new features for two possible factors in degree of heterogeneity of the crust during the Taiwan orogeny. One is the vertical deformation associated with crustal thickening and thinning (Yang & Hauksson 2013) and another is variation in thickness of the crust resulted in different dynamics of mantle flows

(Lin & Kuo 2013). By considering their joint effects on thickened and thinned crust, it may explain that agreement on orientations of stress axes and styles of faulting at the two regimes is not as apparent as in the western Taiwan. The variation of degree of heterogeneity in the vertical space might imply that the brittle part of crust has different strength or thickness depend on evolution of the orogeny. We propose the brittle part of crust could not be considered as constant in strength or depth that was ignored in the layered mechanism (Huang *et al.* 2015). The brittle part of crust is generally regarded as a key constraint for estimate of the characteristic earthquakes on fault segments. In case of the thickness or strength is spatially variable, potential seismic hazard assessments of the earthquakes may be over/underestimated significantly by using geodetic strain rates and seismic stress tensors. We attributed this interpretation to directions of strain and stress axes provide physical meaning is independent of seismic anisotropic structures. Further exploration of our updated data sets and results from strain and stress tensors may reveal more heterogeneity in vertical space of the crust. We highlighted importance of vertical deformation in the orogeny that was difficult to be estimated due to insufficient focal mechanisms at depths for stress inversions. Advanced methods for geodetic strain estimates and seismic stress inversions should be applied to directly understand vertical strain and stress deviations in crustal thickening or thinning orogenies.

5 CONCLUSIONS

This study reassessed geodetic strain-rate tensors of the Taiwan orogen as well as seismic stress tensors from the surface to the depth of 40 km. We estimated the strain-rate tensors in horizontal 0.1° -spacing grids by using updated data of cGPS station velocities of a 21 yr trend. We determined the stress tensors and calculated the $A\phi$ values in a 3-D grid of $0.1^\circ \times 0.1^\circ \times 10 \text{ km}$ based on an updated data set of 25 yr earthquake focal mechanisms. We first minimized effect of the M_w 7.6 Chi-Chi earthquake on estimate of trends of the strain and stress by correcting the cGPS velocities recorded prior to the earthquake and removing the first 15-month focal mechanisms within the fault rupture zone. Our results indicate that internal deformation of the orogenic crust of Taiwan is spatial heterogeneity that is depth-dependent. Directions of the seismic compressive axes are fan-shaped oriented toward 310° in the western and mid-eastern Taiwan at the depths of 0–20 km. The orientations show near parallel to orientations of geodetic compressional axes but most of them have rotated counter-clockwise at the depths of 20–40 km. The variation in orientations of compressive axes coincided with observed transition of styles of faulting from reverse to strike-slip faulting along the depths. The evidences indicate that internal deformation of the orogenic crust is not presently driven by the single mechanism, and geodetic strain field could explain the deformation within the upper crust. Heterogeneity in orientations of seismic compressive axes and styles of faulting is founded to be strong and weak in or near areas of the thickened/thinned and overthickened crust, respectively. The variation in thickness of the crust imply that vertical deformation in the orogeny is crucial to degree of the heterogeneity.

ACKNOWLEDGEMENTS

We wish to thank the Central Weather Bureau for providing the seismic data. The comments and suggestions of the editor and two anonymous reviewers led to significant improvements of the

manuscript. This research was supported by the Ministry of Science and Technology (MOST) of Taiwan. The author gratefully acknowledges Wessel *et al.* (2013) for the Generic Mapping Tool (GMT) software that was used in plotting some of the figures.

REFERENCES

- Altamimi, Z., Collilieux, X. & Métivier, L., 2011. ITRF2008: an improved solution of the terrestrial reference frame, *J. Geod.*, **85**, 457–473.
- Becker, T.W., Hardebeck, J.L. & Anderson, G., 2005. Constraints on fault slip rates of the southern California plate boundary from GPS velocity and stress inversions, *Geophys. J. Int.*, **160**, 634–650.
- Bos, A.G., Spakman, W. & Nyst, M.C.J., 2003. Surface deformation and tectonic setting of Taiwan inferred from a GPS velocity field, *J. geophys. Res.*, **108**(B10), 2458, doi:10.1029/2002JB002336.
- Chan, C.H., Hsu, Y.J. & Wu, Y.M., 2012. Possible stress states adjacent to the rupture zone of the 1999 Chi-Chi, Taiwan, earthquake, *Tectonophysics*, **541–543**, 81–88.
- Chang, C.P., Chang, T.Y., Angelier, J., Kao, H., Lee, J.C. & Yu, S.B., 2003. Strain and stress field in Taiwan oblique convergent system: constraints from GPS observation and tectonic data, *Earth planet. Sci. Lett.*, **214**, 115–127.
- Chen, S.K., Chan, Y.C., Hu, J.C. & Kuo, L.C., 2014. Current crustal deformation at the junction of collision to subduction around the Hualien area, Taiwan, *Tectonophysics*, **617**, 58–78.
- Chiang, P.J., Hsu, Y.J. & Chang, W.L., 2016. Fault modeling of the 2012 Wutai, Taiwan earthquake and its tectonic implications, *Tectonophysics*, **666**, 66–75.
- Ching, K.E., Hsieh, M.L., Johnson, K.M., Chen, K.H., Rau, R.J. & Yang, M., 2011a. Modern vertical deformation rates and mountain building in Taiwan from precise leveling and continuous GPS observations, 2000–2008, *J. geophys. Res.*, **116**, B08406, doi:10.1029/2011JB008242.
- Ching, K.E., Rau, R.J., Johnson, K.M., Lee, J.C. & Hu, J.C., 2011b. Present-day kinematics of active mountain building in Taiwan from GPS observations during 1995–2005, *J. geophys. Res.*, **116**, B09405, doi:10.1029/2010JB008058.
- Dach, R., Hugentobler, U., Fridez, P. & Meindl, M., 2007. *User Manual of Bernese GPS Software Version 5.0*, University of Bern, Bern, Switzerland, p. 640.
- Hardebeck, J.L. & Hauksson, E., 2001. The crustal stress field in southern California and its implications for fault mechanics, *J. geophys. Res.*, **106**, 21 859–21 882.
- Hardebeck, J.L. & Michael, A.J., 2006. Damped regional-scale stress inversions: methodology and examples for southern California and the Coalinga aftershock sequence, *J. geophys. Res.*, **111**, B11310, doi:10.1029/2005JB004144.
- Hasegawa, A., Yoshida, K., Asano, Y., Okada, T., Iinuma, T. & Ito, Y., 2012. Change in stress field after the 2011 great Tohoku-Oki earthquake, *Earth planet. Sci. Lett.*, **355–356**, 231–243.
- Hsieh, H.H. & Yen, H.Y., 2016. Three-dimensional density structures of Taiwan and tectonic implications based on the analysis of gravity data, *J. Asian Earth Sci.*, **124**, 247–259.
- Hsu, Y.J., 2004. Modeling studies on interseismic, coseismic and postseismic deformations associated with the 1999 Chi-Chi, Taiwan earthquake, *PhD thesis*, National Central University, Chungli, Taiwan.
- Hsu, Y.J., Rivera, L., Wu, Y.M., Chang, C.C. & Kanamori, H., 2010. Spatial heterogeneity of tectonic stress and friction in the crust: new evidence from earthquake focal mechanism in Taiwan, *Geophys. J. Int.*, **182**, 329–342.
- Hsu, Y.J., Segall, P., Yu, S.B., Kuo, L.C. & Williams, C.A., 2007. Temporal and spatial variations of postseismic deformation following the 1999 Chi-Chi, Taiwan earthquake, *Geophys. J. Int.*, **169**, 367–379.
- Hsu, Y.J., Yu, S.B., Simons, M., Kuo, L.C. & Chen, H.Y., 2009. Interseismic crustal deformation in the Taiwan plate boundary zone revealed by GPS observations, seismicity, and earthquake focal mechanisms, *Tectonophysics*, **479**, 4–18.
- Hu, J.C., Angelier, J., Lee, J.C., Chu, T.H. & Byrne, D., 1996. Kinematics of convergence, deformation and stress distribution in the Taiwan collision area: 2-D finite-element numerical modelling, *Tectonophysics*, **255**, 243–268.
- Hu, J.C., Yu, S.B., Chu, H.T. & Angelier, J., 2002. Transition tectonics of northern Taiwan induced by convergence and trench retreat, *Spec. Pap. Geol. Soc. Am.*, **358**, 149–162.
- Huang, H.H., Shyu, J.B.H., Wu, Y.M., Chang, C.H. & Chen, Y.G., 2012. Seismotectonics of northeastern Taiwan: kinematics of the transition from waning collision to subduction and postcollisional extension, *J. geophys. Res.*, **117**, B01313, doi:10.1029/2011JB008852.
- Huang, H.H., Wu, Y.M., Song, X.D., Chang, C.H., Lee, S.C., Chang, T.M. & Hsieh, H.H., 2014. Joint V_p and V_s tomography of Taiwan: implications for subduction-collision orogeny, *Earth planet. Sci. Lett.*, **392**, 177–191.
- Huang, T.Y., Gung, Y.C., Kuo, B.Y., Chiao, L.Y. & Chen, Y.N., 2015. Layered deformation in the Taiwan orogeny, *Science*, **349**, 720–723.
- Kao, H. & Jian, P.R., 2001. Seismogenic patterns in the Taiwan region: insights from source parameter inversion of BATS data, *Tectonophysics*, **333**, 179–198.
- Keiding, M., Lund, B. & Árnadóttira, T., 2009. Earthquakes, stress, and strain along an obliquely divergent plate boundary: Reykjanes Peninsula, southwest Iceland, *J. geophys. Res.*, **114**, B09306, doi:10.1029/2008JB006253.
- Ko, Y.T., Kuo, B.Y., Wang, K.L., Lin, S.C. & Hung, S.H., 2012. The southwestern edge of the Ryukyu subduction zone: a high Q mantle wedge, *Earth planet. Sci. Lett.*, **335–336**, 145–153.
- Koulikov, I., Jakovlev, A., Wu, Y.M., Dobretsov, N.L., Khrepy, S.El. & Al-Arifi, N., 2015. Three-dimensional seismic anisotropy in the crust and uppermost mantle beneath the Taiwan area revealed by passive source tomography, *J. geophys. Res.*, **120**, 7814–7829.
- Kuo, B.Y., Wang, C.C., Lin, S.C., Lin, C.R., Chen, P.C., Jang, J.P. & Chang, H.K., 2012. Shear-wave splitting at the edge of the Ryukyu subduction zone, *Earth planet. Sci. Lett.*, **355–356**, 262–270.
- Kuo-Chen, H., Sroda, P., Wu, F.T., Wang, C.Y. & Kuo, Y.W., 2013. Seismic anisotropy of the upper crust in the mountain ranges of Taiwan from the TAIGER explosion experiment, *Terr. Atmos. Ocean Sci.*, **24**, 963–970.
- Kuo-Chen, H., Wu, F.T. & Roecker, S.W., 2012. Three-dimensional P velocity structures of the lithosphere beneath Taiwan from the analysis of TAIGER and related seismic datasets, *J. geophys. Res.*, **117**, B06306, doi:10.1029/2011JB009108.
- Lee, S.J., Ma, K.F. & Chen, H.W., 2006. Three-dimensional dense strong motion waveform inversion for the rupture process of the 1999 Chi-Chi, Taiwan, earthquake, *J. geophys. Res.*, **111**, B11308, doi:10.1029/2005JB004097.
- Lin, K.C. *et al.*, 2010. GPS crustal deformation, strain rate, and seismic activity after the 1999 Chi-Chi earthquake in Taiwan, *J. geophys. Res.*, **115**, B07404, doi:10.1029/2009JB006417.
- Lin, S.C. & Kuo, B.Y., 2013. Trench-parallel flow in the southern Ryukyu subduction system: effects of progressive rifting of the overriding plate, *J. geophys. Res.*, **118**, 302–315.
- Liu, T.K., 1982. Tectonic implication of fission track ages from the Central Range, Taiwan, *Proc. Geol. Soc. China*, **25**, 22–37.
- Nikolaidis, R., 2002. Observation of geodetic and seismic deformation with the global positioning system, *PhD thesis*, University of California, San Diego, USA.
- Palano, M., 2015. On the present-day crustal stresses, strain-rate fields and mantle anisotropy pattern of Italy, *Geophys. J. Int.*, **200**, 967–983.
- Palano, M., Cannavò, F., Ferranti, L., Mattia, M. & Mazzella, E., 2011. Strain and stress fields in the Southern Apennines (Italy) constrained by geodetic, seismological and borehole data, *Geophys. J. Int.*, **187**(3), 1270–1282.
- Rau, R.J., Liang, W.T., Kao, H. & Huang, B.S., 2000. Shear wave anisotropy beneath the Taiwan orogen, *Earth planet. Sci. Lett.*, **177**, 177–192.
- Rousset, B., Barbot, S., Avouac, J.P. & Hsu, Y.J., 2012. Postseismic deformation following the 1999 Chi-Chi earthquake, Taiwan: implication for lower-crust rheology, *J. geophys. Res.*, **117**, B12405, doi:10.1029/2012JB009571.

- Simoes, M., Avouac, J.P., Beyssac, O., Goffé, B., Farley, K.A. & Chen, Y.G., 2007. Mountain building in Taiwan: a thermokinematic model, *J. geophys. Res.*, **112**, B11405, doi:10.1029/2006JB004824.
- Suppe, J., 1981. Mechanics of mountain building and metamorphism in Taiwan, *Mem. Geol. Soc. China*, **4**, 67–89.
- Teng, L.S., 1990. Geotectonic evolution of late Cenozoic arc continent collision in Taiwan, *Tectonophysics*, **183**, 57–76.
- Townend, J. & Zoback, M.D., 2006. Stress, strain, and mountain building in central Japan, *J. geophys. Res.*, **111**, B03411, doi:10.1029/2005JB003759.
- Wang, C.Y., Flesch, L.M., Silver, P.G., Chang, L.J. & Chan, W.W., 2008. Evidence for mechanically coupled lithosphere in central Asia and resulting implications, *Geology*, **36**(5), 363–366.
- Wessel, P., Smith, W.H.F., Scharroo, R., Luis, J.F. & Wobbe, F., 2013. Generic mapping tools: improved version released, *EOS, Trans. Am. geophys. Un.*, **94**(45), 409–420.
- Wesson, R.L. & Boyd, O.S., 2007. Stress before and after the 2002 Denali fault earthquake, *Geophys. Res. Lett.*, **34**, L07303, doi:10.1029/2007GL029189.
- Wu, Y.M. & Chen, C.C., 2007. Seismic reversal pattern for the 1999 Chi-Chi, Taiwan, M_w 7.6 earthquake, *Tectonophysics*, **429**(1–2), 125–132.
- Wu, F.T., Rau, R.J. & Salzberg, D., 1997. Taiwan orogeny: thin skinned or lithospheric collision?, *Tectonophysics*, **274**, 191–220.
- Wu, Y.M., Chang, C.H., Zhao, L., Shyu, J.B.H., Chen, Y.G., Sieh, K. & Avouac, J.P., 2007. Seismic tomography of Taiwan: improved constraints from a dense network of strong motion stations, *J. geophys. Res.*, **112**, B08312, doi:10.1029/2007JB004983.
- Wu, Y.M., Chang, C.H., Zhao, L., Teng, T.L. & Nakamura, M., 2008a. A comprehensive relocation of earthquakes in Taiwan from 1991 to 2005, *Bull. seism. Soc. Am.*, **98**(3), 1471–1481.
- Wu, Y.M., Zhao, L., Chang, C.H. & Hsu, Y.J., 2008b. Focal mechanism determination in Taiwan by genetic algorithm, *Bull. seism. Soc. Am.*, **98**(2), 651–661.
- Wu, F.T., Liang, W.T., Lee, J.C., Benz, H. & Villasenor, A., 2009. A model for the termination of the Ryukyu subduction zone against Taiwan: a junction of collision, subduction/separation, and subduction boundaries, *J. geophys. Res.*, **114**, B07404, doi:10.1029/2008JB005950.
- Wu, W.N., Kao, H., Hsu, S.K., Lo, C.L. & Chen, H.W., 2010a. Spatial variation of the crustal stress along the Ryukyu-Taiwan-Luzon convergence boundary, *J. geophys. Res.*, **115**, B11401, doi:10.1029/2009JB007080.
- Wu, Y.M., Hsu, Y.J., Chang, C.H., Teng, L.S. & Nakamura, M., 2010b. Temporal and spatial variation of stress field in Taiwan from 1991 to 2007: insights from comprehensive first motion focal mechanism catalog, *Earth planet. Sci. Lett.*, **298**, 306–316.
- Wu, Y.M., Chang, C.H., Kuo-Chen, H., Huang, H.H. & Wang, C.Y., 2013. On the use of explosion records for examining earthquake location uncertainty in Taiwan, *Terr. Atmos. Ocean. Sci.*, **24**, 685–694.
- Yang, W. & Hauksson, E., 2013. The tectonic crustal stress field and style of faulting along the Pacific North America Plate boundary in Southern California, *Geophys. J. Int.*, **194**, 100–117.
- Yoshida, K., Hasegawa, A., Okada, T., Iinuma, T., Ito, Y. & Asano, Y., 2012. Stress before and after the 2011 great Tohoku-oki earthquake and induced earthquakes in inland areas of eastern Japan, *Geophys. Res. Lett.*, **39**, L03302, doi:10.1029/2011GL049729.
- Yu, S.B., Chen, H.Y. & Kuo, L.C., 1997. Velocity field of GPS stations in the Taiwan area, *Tectonophysics*, **274**, 41–59.
- Yu, S.B., Hsu, Y.J., Kuo, L.C., Chen, H.Y. & Liu, C.C., 2003. GPS measurement of postseismic deformation following the 1999 Chi-Chi, Taiwan, earthquake, *J. geophys. Res.*, **108**(B11), 2520, doi:10.1029/2003JB002396.

SUPPORTING INFORMATION

Supplementary data are available at [GJI](#) online.

Figure S1. Locations of 7 surrounding IGS sites and 12 local cGPS sites of Taiwan. The study area is marked by a black rectangle and enlarged in the left-bottom corner.

Figure S2. Examples of test results from random removal of 10 per cent of cGPS sites (see the main text).

Figure S3. Depth distribution of earthquake focal mechanisms of Taiwan from 1991 to 2015 used in this study.

Figure S4. The amount of focal mechanisms within each grid cell for the stress tensor inversion.

Please note: Oxford University Press is not responsible for the content or functionality of any supporting materials supplied by the authors. Any queries (other than missing material) should be directed to the corresponding author for the paper.